 CMES, vol.58, no.3, pp.247-270, 2010

Analysis of a Crack in a Thin Adhesive Layer between Orthotropic Materials: An Application to Composite Interlaminar Fracture Toughness Test

L. Távara,[1] V. Mantič,[1] E. Graciani,[1] J. Cañas[1] and F. París[1]

Abstract: The problem of a crack in a thin adhesive layer is considered. The adherents may have orthotropic elastic behavior which allows composite laminates to be modeled. In the present work a linear elastic-brittle constitutive law of the thin adhesive layer, called weak interface model, is adopted, allowing an easy modeling of crack propagation along it. In this law, the normal and tangential stresses across the undamaged interface are proportional to the relative normal and tangential displacements, respectively. Interface crack propagation is modeled by successive breaking of the springs used to discretize the weak interface. An important feature of the BEM approach developed is that the behavior of the springs is independent of the boundary element mesh, (i.e. distance between springs and boundary element types used). This fact allows, for example, an easy mesh refinement to be performed. The present model allows not only the crack propagation but also the crack initiation to be studied. The problem of two linear elastic half-planes bonded by a cracked thin adhesive layer is considered first. A formulation of the new governing integral equation for two identical orthotropic half-planes bonded along a straight weak interface including a finite interface crack under constant pressure is presented, introducing a new dimensionless characteristic structural parameter δ. A parametric study of this problem by BEM is presented, verifying the correct implementation of the weak interface model. Then, the Interlaminar Fracture Toughness (G_{Ic}) Test is analyzed by the BEM code developed. The crack propagation is studied by a new Energy Release Rate criterion. It is shown that the weak interface model of the adhesive layer, used in the 2D Boundary Element Method (BEM) code developed, provides a good representation of the actual adhesive behavior by comparing numerical and experimental results.

Keywords: crack, BEM, delamination, adhesive layer, imperfect interface, weak interface, spring boundary condition, composites, DCB.

[1] Escuela Técnica Superior de Ingenieros, University of Sevilla, Camino de los Descubrimientos s/n, Sevilla 41092, Spain.

1 Introduction

The majority of methods used to simulate crack propagation, based on the classical Linear Elastic Fracture Mechanics (LEFM), made difficult the study of crack initiation occurring in the first step of fracture process, since they assume the presence of a crack. Recently, other models have been intensively developed, like energetically based delamination model [Kočvara, Mielke, and Roubíček (2006); Roubíček, Scardia, and Zanini (2009)] or cohesive crack models [Hilleborg, Modeer, and Petersson (1976); Needleman (1987); Carpinteri (1989a); Carpinteri (1989b); Camacho and Ortiz (1996); Maier and Frangi (1998); Camanho, Dávila, and de Moura (2003)]. In particular, cohesive crack models assume hypotheses different to those adopted in LEFM avoiding the presence of stress singularity at the crack tip. These models are suitable to study both the crack initiation and crack propagation, and also to estimate the fracture energy by suitable tests, and subsequently the maximum allowable load of a structure.

In many practical situations, the behavior of adhesive joints can be described modeling the thin adhesive layer as a continous distribution of linear elastic springs [Erdogan (1997)] with appropriate stiffness parameters. This model of adhesive layer is usually called weak interface or elastic interface [Geymonat, Krasucki, and Lenci (1999); Lenci (2001)]. In the present work a linear elastic-brittle constitutive law is adopted for the springs representing the weak interface in order to allow an easy modeling of crack propagation along the interface. This weak interface model has been implemented in a 2D BEM code [París and Cañas (1997); Graciani, Mantič, París, and Blázquez (2005)], whose original version allowed isotropic axisymmetric and anisotropic plane problems to be modeled, including multiple solids with strong interfaces (perfectly bonded) or contact zones between them. The new feature incorporated in this code is the possibility of defining weak interfaces between the elastic solids. It is noteworthy that the BEM is a suitable tool for modeling a crack growing along the weak interface because the non-linearity introduced is associated only to the interface boundary. Another feature of the code is that the equilibrium and compatibility conditions, along contact zones and along strong or weak interfaces, are imposed in a weak form allowing an easy use of non-conforming discretizations [Blázquez, París, and Mantič (1998); Graciani, Mantič, París, and Blázquez (2005)].

A good understanding and characterization of the adhesive layer behavior is very important in the quality evaluation of adhesively bonded joints, and particularly in determining the parameters that characterize their resistance to fracture and failure. These parameters can then be used in the design and quality control of the production processes. The quality of an adhesive joint between composite laminates is usually evaluated by an Interlaminar Fracture Toughness Test, where an

estimation of the critical interlaminar fracture energy (G_{Ic}) is obtained. Extensive experimental and numerical studies by Finite Element Method of this test (using different adhesives) have recently been carried out by the present authors and their co-workers, see [Távara, Mantič, Graciani, Cañas, and París (2008); Távara, Mantič, Graciani, Cañas, and París (2009)] and references therein.

2 Weak interface

2.1 Constitutive law of spring distribution

According to [Erdogan (1997); Geymonat, Krasucki, and Lenci (1999); Lenci (2001); Carpinteri, Cornetti, and Pugno (2009)], a weak interface is considered as a simple and useful model of a thin linear elastic adhesive layer between two surfaces. The undamaged adhesive layer, considered as a linear elastic solid of Young modulus E_{adh} of width w and small thickness h, can be modeled by a spring distribution.

It is useful to clarify relations between the adhesive layer parameters (E_{adh}, h, w) and the spring stiffness parameters used when the spring constitutive law is written in terms of a force-displacement law, $F - \delta_n$, (typically in an FEM model the relation between the nodal forces and displacements) or in terms of a normal traction-displacement law, $\sigma - \delta_n$, (typically in a BEM model). Considering a portion of the adhesive layer given by a prismatic block of section Lw and height h, see Fig. 1, with L being the distance between the springs, the following form of the force-displacement constitutive law is easily obtained as:

$$F = K_{adh}\delta_n, \quad \text{where} \quad K_{adh} = \frac{E_{adh}Lw}{h}, \tag{1}$$

and of the normal traction-displacement law as:

$$\sigma = k_n\delta_n, \quad \text{where} \quad k_n = \frac{K_{adh}}{Lw} = \frac{E_{adh}}{h}. \tag{2}$$

According to Eq. 1, the stiffness parameter in the force-displacement law depends on the distance L between springs, whereas the stiffness parameter k_n in the traction-displacement law, in Eq. 2, is independent of this distance. Thus, an application of non-uniform meshes, and in particular an adaptive mesh refinement, is much easier to implemented for a spring distribution governed by a traction-displacement law (where the parameter k_n is not affected by the mesh size) than for that governed by a force-displacement law (where the parameter K_{adh} depends on the adjacent element sizes). It is noteworthy to notice that considering very thin adhesive layers with vanishing thickness, $h \to 0$, a constant value of k_n implies, view Eq. 2, vanishing values of the Young modulus, $E_{adh} \to 0$, whereas constant values of E_{adh} imply increasing values of k_n, $k_n \to \infty$.

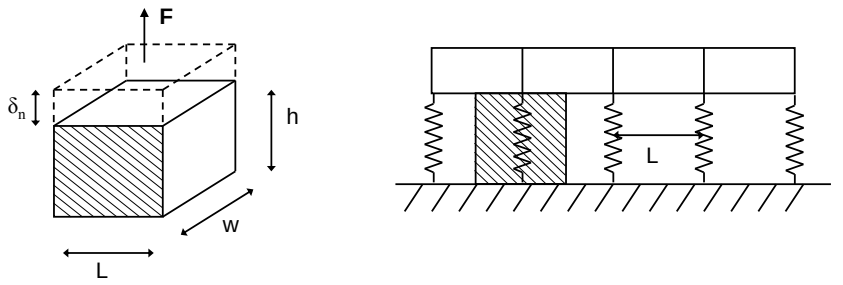

(a) (b)

Figure 1: (a) Portion of the adhesive layer, (b) spring distribution (distance L between springs, FEM model)

2.2 Linear-elastic brittle law of the interface

In the present work, adhesive damage and/or rupture of the thin linear elastic adhesive layer have been modeled as an abrupt free separation of both surfaces when a threshold normal stress, σ_c, is achieved in the layer. Thus, the continuous spring distribution that models the adhesive layer is governed by the following simple linear elastic-brittle law, shown also in Fig. 2:

$$\begin{array}{ll} \text{Linear elastic} & \left\{ \begin{array}{l} \sigma(x) = k_n \delta_n(x) \\ \tau(x) = k_t \delta_t(x) \end{array} \right. \quad \delta_n^*(x) \leq \delta_{nc} \\ \text{interface} & \\ & \\ \text{Broken} & \left\{ \begin{array}{l} \sigma(x) = 0 \\ \tau(x) = 0 \end{array} \right. \quad \delta_n^*(x) > \delta_{nc} \\ \text{interface} & \end{array} \tag{3}$$

where δ_n^* is the maximum normal relative displacement achieved in the spring (which corresponds to an interface point) up to the considered instant of the problem evolution, σ and τ are the normal and tangential stresses respectively in the spring, and δ_n and δ_t are the normal and tangential relative displacements between the spring ends. Sometimes δ_n and δ_t are referred to as the value of the opening and sliding between the interface sides. k_n is the above defined normal stiffness, k_t is the tangential stiffness of the continuous spring distribution, which can be obtained by a similar analysis to that shown above for k_n. Finally σ_c and δ_{nc} are, respectively, the critical normal tension and opening displacement reached when the spring breaks in mode I.

Notice that the springs break when the normal opening δ_n reaches its critical value, δ_{nc}. Therefore, if $\delta_n^*(x) \leq \delta_{nc}$ loading and unloading takes place following the linear elastic law in Eq. 3. When $\delta_n^*(x) > \delta_{nc}$ both normal and tangential stiffness are set to zero (during loading and unloading). This is due to the interface failure criteria assumed herein and explained in the following.

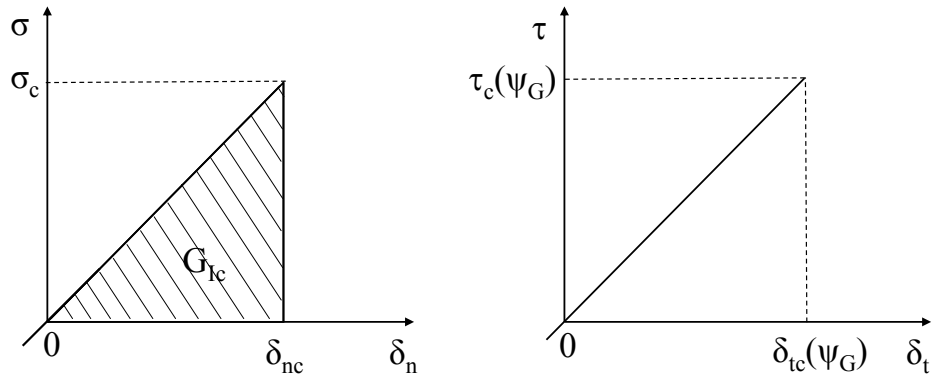

(a) (b)

Figure 2: Normal and tangential linear elastic-brittle law

The interface failure criterion, proposed here, is based on the Energy Release Rate (ERR) concept. The ERR is defined as the stored energy in the unbroken spring situated at the crack tip as shown by [Lenci (2001)] and recently independently also by [Carpinteri, Cornetti, and Pugno (2009)]. Thus, the ERR of a crack in a weak interface is defined as:

$$G = G_I + G_{II} = \frac{\sigma \delta_n}{2} + \frac{\tau \delta_t}{2}, \tag{4}$$

where σ and τ are stresses at the crack tip and δ_n and δ_t are relative displacements at the crack tip. This spring breaks when the crack propagates across it. The total ERR of a crack growing in mixed mode can be defined as:

$$G = G_I + G_{II} = G_I(1 + \tan^2 \psi_G), \tag{5}$$

where

$$\tan^2 \psi_G = \frac{G_{II}}{G_I}, \tag{6}$$

with ψ_G being the angle that defines fracture mode mixity. Thus $\psi_G = 0^\circ$ defines a pure fracture mode I (opening mode) and $\psi_G = 90^\circ$ defines a pure fracture mode II (shear mode) [Evans, Rühle, Dalgleish, and Charalambides (1990); Mantič, Blázquez, Correa, and París (2006)].

In this work a single mode I fracture criterion is adopted. It is assumed that a crack propagates when the ERR associated to mode I, G_I, reaches the mode I fracture energy, that is:

$$G_I = G_{Ic}, \quad \text{where} \quad G_{Ic} = \frac{\sigma_c \delta_{nc}}{2} = \frac{\sigma_c^2}{2k_n} = \frac{k_n \delta_{nc}^2}{2}. \tag{7}$$

Writing the crack propagation criterion along a weak interface as $G = G_c(\psi_G)$ and making use of Eq. 5 and Eq. 7, the following expression of the fracture energy (representing the fracture toughness) as a function of the angle ψ_G is obtained:

$$G_c = G_{Ic}(1 + \tan^2 \psi_G). \tag{8}$$

This expression reminds the fracture toughness law at interfaces studied by [Bank-Sills and Ashkenazi (2000)], although it has been used in a different framework. It is a simple approximation of the experimentally observed behavior of G_c in interface cracks [Liang and Liechti (2005); Swadener, Liechti, and de Lozanne (1999); Bank-Sills and Ashkenazi (2000); Dollhofer, Beckert, Lauke, and Schneider (2001); Agrawal and Karlsson (2007); Mantič (2008)]. The growth of G_c with the increasing angle ψ_G, i.e. increasing participation of shear mode seems to be induced by several phenomena, e.g. localized plasticity at the crack tip and roughness at the crack faces.

As mentioned before, in the present work we use a single mode I fracture criterion. Nevertheless the variables δ_{tc} and τ_{tc}, shown in Fig. 2, can be expressed in terms of δ_{nc}, σ_c and ψ_G, with the following relations:

$$\delta_{tc} = \tan \psi_G \sqrt{\frac{k_n}{k_t}} \delta_{nc}, \tag{9}$$

$$\tau_c = \tan \psi_G \sqrt{\frac{k_t}{k_n}} \sigma_c. \tag{10}$$

A numerical analysis of a mixed mode propagation is presented in Section 5, in order to see the capability of the criterion proposed herein.

3 Weak interface model in the 2D BEM code

3.1 Incremental formulation

The numerical solution of the non-linear problem formulated is based on a gradual application of the loads and displacements imposed, by means of a load factor, $0 \leq \lambda \leq 1$. The solution procedure is given by a series of lineal stages, "load steps". At the beginning of each load step an actual adhesive layer bonded zone is established, which defines the actual linear system of equations. By solving this system the corresponding elastic solution is obtained. Thus, the solution of the

problem will be divided into a number M (a priori unknown) of load steps where the values of the problem variables vary linearly:

$$\phi(x,\lambda) = \lambda \triangle_m \phi(x), \tag{11}$$

with $\lambda_{m-1} \leq \lambda \leq \lambda_m$, $m = 1,...,M$, and $\lambda_0 = 0$, and where $\phi(x,\lambda)$ is the value of any problem variable at a point x after a λ fraction of the load is applied. $\triangle_m \phi(x)$ is the value of the increment of the variable $\phi(x)$ corresponding to the unit increment of the load factor λ, and it is obtained in the solution of the linear system of equations corresponding to the m-th load step. This solution fulfills all the conditions of the weak interface formulation (and also of the contact formulation) up to a certain maximum value λ_m of the load factor λ associated to this load step. A further increment of the load factor leads to rupture of some springs (or to a change in contact conditions). Consequently values of variable ϕ at the end of each load step are defined as $\phi(x,\lambda_m) = \lambda_m \triangle_m \phi(x)$ for $m = 1,...,M$. This procedure is illustrated in Fig. 3.

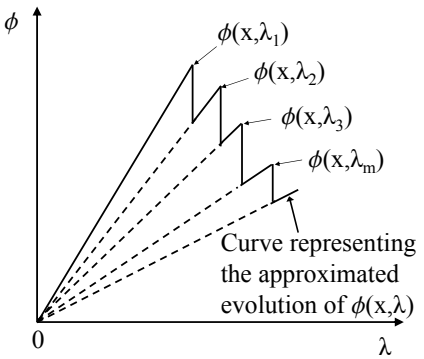

Figure 3: Example of evolution of a variable $\phi(x,\lambda)$

3.2 Linear boundary conditions

The boundary conditions corresponding to the m-th load step are imposed at the nodes of one side of the undamaged weak interface (denoted as A boundary) in the following form (see Eq. 3):

$$\triangle_m t_n^A(x) = k_n \triangle_m \delta_n^A(x), \qquad \triangle_m t_t^A(x) = k_t \triangle_m \delta_t^A(x), \tag{12}$$

where $t_n^A(x)$ are the normal tractions, $\delta_n^A(x)$ are the relative normal displacements (separations of the boundary A with respect to the other boundary denoted as B), $t_t^A(x)$ are the tangential tractions, and $\delta_t^A(x)$ are the relative tangential displacements (slidings of the boundary A with respect to the boundary B). The tangential tractions $t_t^A(x)$ can be taken as zero if a pure mode I problem is considered.

3.3 Non-linear boundary conditions

When solving the m-th load step, the values $\lambda_m^*(x)$ of the load factor that leads to the violation of the condition $G > G_c$ are determined at each interface node, and subsequently the limit load factor of the current step, $\lambda_m = \min \lambda_m^*(x)$, is defined. In the next load step the linear system is defined by replacing in the first node that failed the boundary conditions defined in Eq. 12 by the conditions:

$$\triangle_{m+1} t_n^A(x) = 0, \qquad \triangle_{m+1} t_t^A(x) = 0. \tag{13}$$

This procedure can be repeated as many times as necessary to reach equilibrium after the whole load is applied.

4 Pressurized crack at a weak interface between identical orthotropic half planes

4.1 Governing integral equations

To solve the problem of two isotropic half-planes bonded by a thin adherent layer modeled by a weak interface including a crack and subjected to a far field tension, see Fig. 4(b), Lenci deduced a governing integral equation for the problem of pressurized cracks, see Fig. 4(b), related to the original problem by superposition with a constant stress solution [Lenci (2001)]. The integral equation obtained was solved by a specific numerical procedure.

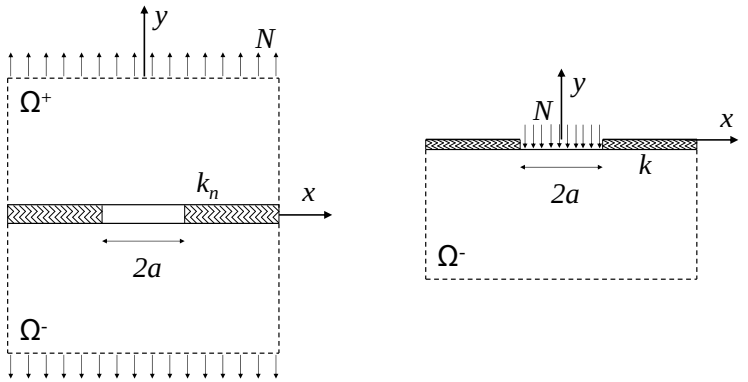

(a) (b)

Figure 4: (a) Crack at a weak interface under far field tension, (b) simplified problem of a pressurized crack at a weak interface.

In this section Lenci's approach will be generalized to the case of identical orthotropic half-planes bonded by a weak interface including a crack and subjected

to far field tension, see Fig. 4(a). Orthotropic axes of adherents are considered parallel and perpendicular to the interface.

Let $\sigma_y(x) = \sigma_y(x, y = 0)$ and $v(x) = v(x, y = 0)$ be the normal stress and the vertical displacement of the lower half-plane at the interface, respectively. By superposition with the constant stress solution $\sigma_y = N$ constant tension $(N > 0)$, and by symmetry with respect to the x-axis we can limit the present analysis to Ω^- subjected to $\sigma_y(x) = -N$ in $|x| < a$, $\sigma_y(x) = -kv(x)$ in $|x| > a$ and $\tau_{xy}(x, y = 0) = 0$, defining the pressurized crack problem shown in Fig. 4(b); $k = 2k_n$ is defined to simplify the notation.

In the case of an isotropic material, by using the Flamant solution as a Green function, the normal stress and the vertical displacement at the upper boundary $(y = 0)$ of Ω^- can be related by [Lenci (2001)]:

$$v(x) = -\frac{\kappa+1}{4\mu\pi} \int_{-\infty}^{+\infty} \sigma_y(t) \ln|t-x| dt, \tag{14}$$

where $\kappa = 3 - 4\nu$ in the case of plane strain and $\kappa = (3-\nu)/(1+\nu)$ in the case of generalized plane stress. The function $\sigma_y(x)$ is even and given by

$$\sigma_y = \begin{cases} -N, & 0 < x < a, \\ G(x), & x > a, \end{cases} \tag{15}$$

where $G(x)$ is the unknown interface stress. The notation introduced by [Lenci (2001)] has been kept in the present paper for an easy comparison of the deduction introduced therein and the present analysis.

In the present case of orthotropic half planes, the strain-stress law for a generalized plane strain state can be expressed in the following way:

$$\begin{pmatrix} \varepsilon_{xx} \\ \varepsilon_{yy} \\ 2\varepsilon_{xy} \end{pmatrix} = \begin{pmatrix} s'_{11} & s'_{12} & 0 \\ s'_{12} & s'_{22} & 0 \\ 0 & 0 & s'_{66} \end{pmatrix} \cdot \begin{pmatrix} \sigma_{xx} \\ \sigma_{yy} \\ \sigma_{xy} \end{pmatrix}, \qquad s'_{IJ} = s_{IJ} - \frac{s_{I3}s_{3J}}{s_{33}}, \tag{16}$$

where s'_{IJ} are the reduced elastic compliances. Applying the concept of the Airy stress function and using Eq. 16, the strain compatibility equation yields the following characteristic equation of an orthotropic material [Lekhnitskii (1981); Ting (1996)].

$$\ell_4(p) = s'_{11}p^4 + (2s'_{12} + s'_{66})p^2 + s'_{22} = 0, \tag{17}$$

whose complex conjugate roots p_α and $\overline{p}_\alpha$ $(\alpha = 1,2)$ can be expressed as [Mantič and París (1995); Blázquez, Mantič, París, and McCartney (2008)]:

$$p_\alpha = \frac{\pm s_- + i s_+}{\sqrt{2 s'_{11}}}, \qquad s_\pm = \sqrt{\sqrt{s'_{11} s'_{22}} \pm (s'_{12} + 0.5 s'_{66})}. \tag{18}$$

By particularizing a general expression for displacement solution in an orthotropic half-plane ($y \leq 0$) subjected to a normal point force (P_y) at its boundary, at the origin of cartesian coordinates ($x = y = 0$), deduced in [Wen (1992)], see also [Lekhnitskii (1981);Ting (1996)], the following simple expression of normal displacements along the half-plane boundary ($y = 0$) originated by this force can be obtained:

$$v(x) = -\frac{s_+ \sqrt{s'_{22}} P_y}{\pi} \ln |x|. \tag{19}$$

Thus, in a similar way as in Eq. 14, we can define for the case of an orthotropic half-plane bonded by a weak interface, as shown in Fig. 4(b), the vertical displacement of the bottom side of the interface as

$$v(x) = -\frac{s_+ \sqrt{s'_{22}}}{\pi} \int_{-\infty}^{+\infty} \sigma_y(t) \ln |t - x| dt. \tag{20}$$

Then, using Eq. 15 and Eq. 20 and introducing dimensionless coordinates $r = t/a$ and $\xi = x/a$ yields:

$$v(\xi) = -\frac{s_+ \sqrt{s'_{22}}}{\pi} aN \left\{ 2 \ln a \int_1^\infty g(r) dr + \int_1^\infty g(r) \ln |r^2 - \xi^2| dr - 2 \ln a + h(\xi) \right\}, \tag{21}$$

where

$$h(\xi) = -\ln \left| \xi^2 - 1 \right| + \xi \ln \left| \frac{\xi - 1}{\xi + 1} \right| + 2, \tag{22}$$

and $g(r) = G(ar)/N = G(t)/N$ is the unknown dimensionless stress along the bonded interface part. In the problem illustrated in Fig. 4(b), the vertical displacement $v(x)$ vanishes when $x \to \infty$ and the sum of the forces applied to Ω^- is zero. Consequently, the global equilibrium condition takes the form:

$$\int_1^\infty g(r) dr = 1. \tag{23}$$

Eq. 21 can be simplified, by substituting Eq. 23, into the following form:

$$v(\xi) = -\frac{s_+\sqrt{s'_{22}}}{\pi} aN \left\{ \int_1^\infty g(r) \ln|r^2 - \xi^2| dr + h(\xi) \right\}. \tag{24}$$

In the joined part $\xi > 1$, the vertical displacement satisfies the weak interface condition $\sigma_y(\xi) = -kv(\xi)$. This relationship and Eq. 24 finally give the integral equation which governs the problem:

$$g(\xi) = \delta \left\{ \int_1^\infty g(r) \ln|r^2 - \xi^2| dr + h(\xi) \right\}, \qquad \xi > 1, \tag{25}$$

where

$$\delta = \frac{s_+\sqrt{s'_{22}} ka}{\pi} \tag{26}$$

is a new dimensionless parameter governing the pressurized crack solution at a weak interface between orthotropic materials. It is a structural parameter because it relates adhesive-layer stiffness to the adherent stiffness, taking into account the crack length (the unique characteristic length of the geometry of the present problem).

Note that the present dimensionless form of the governing integral equation in Eq. 25 coincides with that obtained by [Lenci (2001)] except for the present definition of δ for orthotropic half-planes bonded by a cracked weak interface. The present definition of δ is in fact a generalization of Lenci's original isotropic definition to the general orthotropic case. It can be shown that Eq. 26 when written for isotropic materials reduces to Lenci's expression $\delta = ka(\kappa+1)/(4\pi\mu)$.

4.2 Numerical solution

The numerical solution of the problem defined in the previous section (Fig. 4) is obtained here by using a collocational BEM code [París and Cañas (1997); Graciani, Mantič, París, and Blázquez (2005)], solving the Somigliana displacements identity for orthotropic materials. This code uses linear continous elements [París and Cañas (1997)] for both elastic plane and axisymmetric problems.

To solve the problem of pressurized cracks in a weak interface between two orthotropic half-planes, the problem symmetry with respect to the y-axis has been used. Each half-plane has been modeled by a square domain much larger than the crack size, trying to simulate a finite crack between infinite half-planes. The mesh

used for each square domain has 518 elements. The height and width of each square domain is 100 times the size of the crack half-length a (taken as 1mm herein), see Fig. 4(a).

According to Section 4.1 the dimensionless form of the solutions of a pressurized crack at a weak interface between orthotropic and isotropic half planes coincides. The orthotropic material properties used in BEM calculations are those of an 8552/AS4 carbon fiber - epoxy composite that will be defined in Section 5. Nevertheless, as the numerical results obtained are presented in dimensionless form, they are valid for any orthotropic material. Then, in order to obtain the different values of the dimensionless parameter δ shown, the value k was varied from 109.8 x 10^9 Pa/m to 109.8 x 10^{13} Pa/m.

The numerical results for orthotropic materials obtained by the BEM code (when changed to dimensionless form and using the new characteristic parameter δ, defined in Eq. 26) are in excellent agreement with those obtained for isotropic materials in [Lenci (2001)] by a different numerical procedure, solving the equation corresponding to Eq. 25 herein.

The function $g(\xi)$ is reported in Fig. 5(a) for different values of δ. For relatively "soft" interfaces (i.e., low values of δ) $g(\xi)$ achieves very small and almost constant values, while in the opposite case of "stiff" interfaces the stresses are mostly different from zero only in the neighborhood of the crack tip. To better visualize the shape of the solution, the normalized function $g(\xi)/g(1)$ is shown in Fig. 5(b), which illustrates for example how slowy the solution spreads over the whole interface when δ tends to zero.

An important feature of the solution shown in [Lenci (2001)] is its behavior near the crack tip, where interface tractions are bounded at the tip of a crack situated along a weak interface, in contrast with the singular (unbounded) tractions at the tip of an interface crack situated along a perfect interface (also called strong interface, where no relative displacements of bonded surfaces are allowed). Thus, during crack growth along a weak interface, tractions are kept bounded. It appears that local normal tractions in the zone close to the interface crack tip follow the asymptotic law [Lenci (2001)]:

$$\sigma \cong \sigma_0 + \sigma_1 \xi \left[\ln(\xi) - 1\right], \quad \text{for} \quad \xi \to 0_+. \tag{27}$$

The vertical displacement $v(\xi)$ at the bottom side of the interface is depicted in Fig. 5(c). It has a minimum in the midpoint of the crack and it monotonically tends to zero when $\xi \to \infty$. For "soft" interfaces the displacement is large (tending to infinity as $\delta \to 0$), while for "stiff" interfaces it rapidly converges to the Griffith crack displacements. From observation it can be concluded that for $\delta > 100$ the

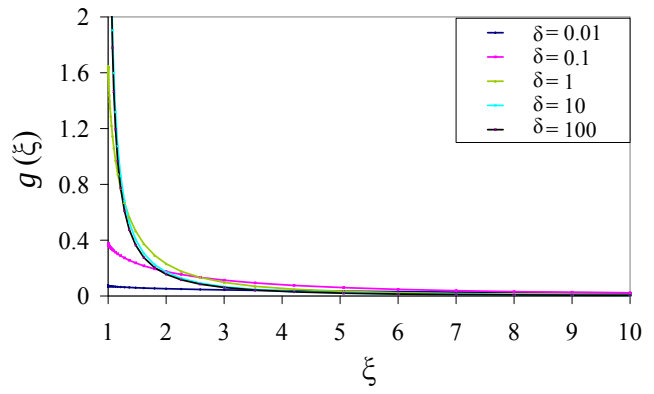

(a)

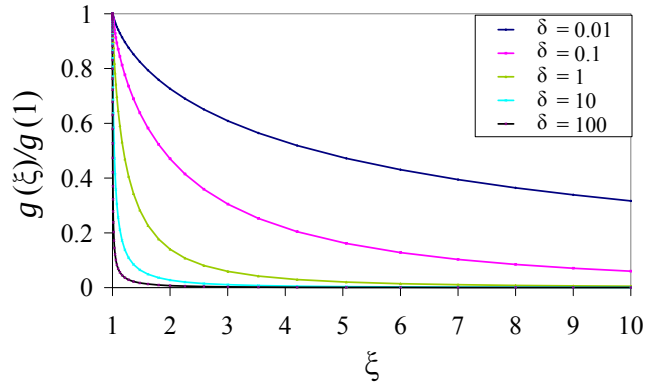

(b)

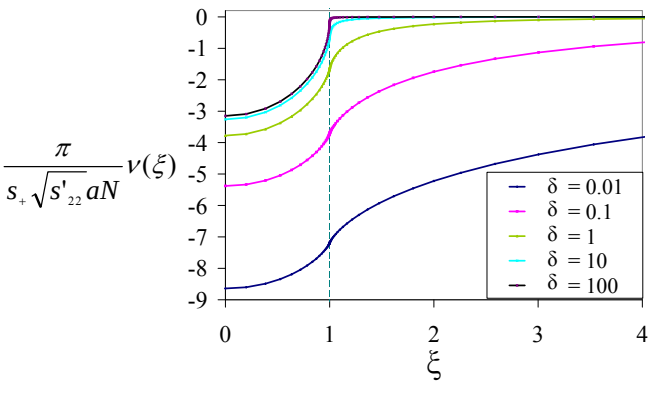

(c)

Figure 5: Pressurized crack at a weak interface between identical orthotropic half-planes. BEM solution for various values of the parameter δ: (a) function $g(\xi)$, (b) normalized solution $g(\xi)/g(1)$, and (c) normalized vertical displacement $v(\xi)$.

weak interface can be considered as a perfect bonding for practical purposes. An excellent agreement of the present results for orthotropic materials in their dimensionless form with those presented by [Lenci (2001)] for isotropic materials has been obtained. Recall that Lenci solved Eq. 25 for isotropic materials by a special numerical procedure, whereas in the present work the two Somigliana displacement identities for the upper and bottom orthotropic adherents have been solved by the collocational BEM.

5 Interlaminar fracture toughness tests

5.1 Laboratory test description

The tests used in the aeronautical industry to evaluate the interlaminar fracture toughness in composite-composite joints are performed by well-known standard procedures [Airbus (2006); ISO (2001)].

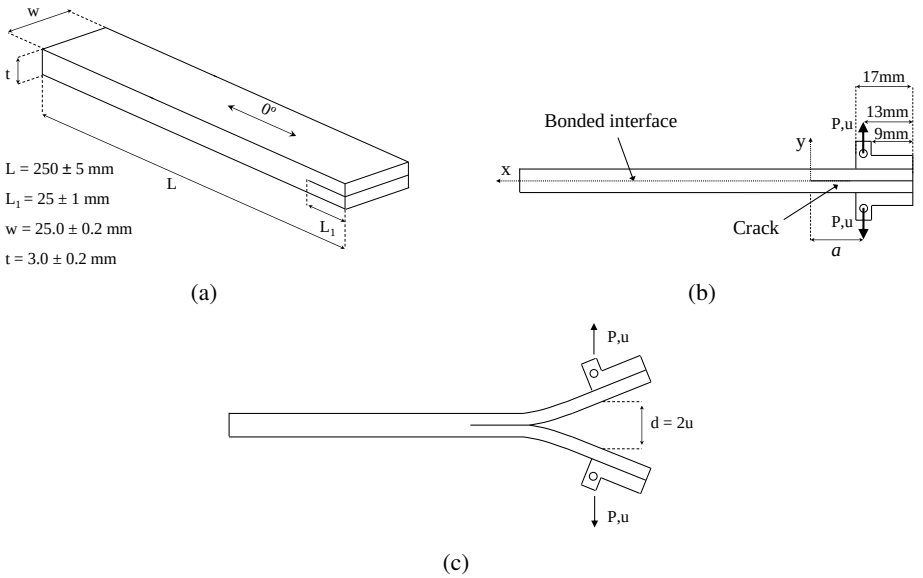

Figure 6: (a) Scheme of the DCB specimen, (b) DCB specimen with bonded tabs, (c) test configuration.

The specimen used is the Double Cantilever Beam (DCB) shown in Fig. 6(a). The DCB specimen is formed by two laminates joined by a thin adhesive layer. The laminates are processed according to EN 2565 standard, and the specimens are cut after the panel has been cured. The specimen is connected to the grips of a universal testing machine through small tabs bonded to laminates as shown in Fig. 6(b). The load (P) and the relative displacement (d) of the wedge grips are continuously

registered during crack propagation, Fig. 6(c).

In a study of the experimental results obtained from G_{Ic} tests and fractographic analysis, using different kinds of adhesive, it was observed that some adhesives like FM 300K0.5 and EA 9695 K.05 presented jumps (non-smooth behavior) in the experimental load-displacement curve. This behavior seems to be explained by the presence of a polyester support in these adhesives [Jiménez, Cañas, Mantič, and Ortiz (2007); Távara, Mantič, Graciani, Cañas, and París (2008); Távara, Mantič, Graciani, Cañas, and París (2009)].

Figure 7: Fracture surface of a G_{Ic}-specimen tested with EA 9695 K.05 adhesive.

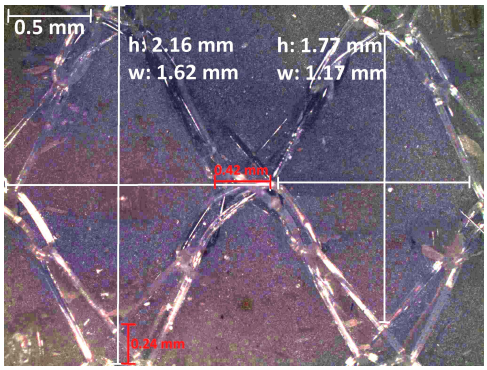

Figure 8: Detail of the polyester support of the EA 9695 K.05 adhesive, outer and inner dimensions of the rhombus-like mesh. Picture taken at 50x zoom.

In Fig. 7 the fracture surface of a tested G_{Ic} specimen with EA 9695 K.05 adhesive is shown. Worthy of note are observe the clearly visible marks on the specimen fracture surface that are related to the jumps appearing in the experimental load - displacement curve. At initial stages, the distance between marks is shorter than at further stages, resulting in larger jumps. In Fig. 8 a detailed picture, taken at 50x zoom, of the polyester support of the adhesive is shown.

5.2 Numerical results

In the present numerical study, a plane strain model has been solved using the BEM code described above, assuming the hypothesis of small strains. The laminate considered is an 8552/AS4 carbon fiber - epoxy composite (having only 0º plies), with the following orthotropic properties: E_x=135GPa, E_y=10GPa, E_z=10GPa, G_{xy}=5GPa, G_{xz}=5GPa, ν_{xy}=0.3, ν_{yz}=0.4 and ν_{xz}=0.3. The adhesive used is EA 9695 K.05, an

epoxy adhesive with a polyester mesh support. The estimated properties of the adhesive spring model are: k_n=150GPa/m, σ_c =15MPa and δ_{nc}=0.1mm, see Fig. 2. A load P was progressively applied at both laminates in the direction normal to the specimen boundary at a distance 13mm from the extreme where the initial crack is situated, see Fig. 6(b). Two point supports were defined at the left-hand extreme of the specimen, Fig. 6(b,c), to remove the rigid body motion in the displacement solution by the use of the method described in [Blázquez, Mantič, París, and Cañas (1996)]

The normal stresses along the bonded zone obtained in a load step corresponding to the decreasing part of the load-displacement curve with P=29.7N, d=0.0354m and a=146.6mm (using two different meshes), are shown in Fig. 9. The initial length of the adhesive layer (225 mm) is discretized by means of 468 (coarse mesh) or 936 (fine mesh) springs placed between the nodes of the conforming boundary element meshes on the upper and bottom sides of the weak interface. As can be observed in Fig. 9, a very accurate solution has already been obtained by the coarse mesh. The corresponding analytical solution of Strength of Materials for a beam on Winkler elastic-foundation deduced in [Kanninen (1973)][1] (Eq. 4 therein) has also been included in Fig. 9. The agreement between this analytic solution and the present BEM solution is good, significant differences being observed only in the zone close to the crack tip, as could be expected.

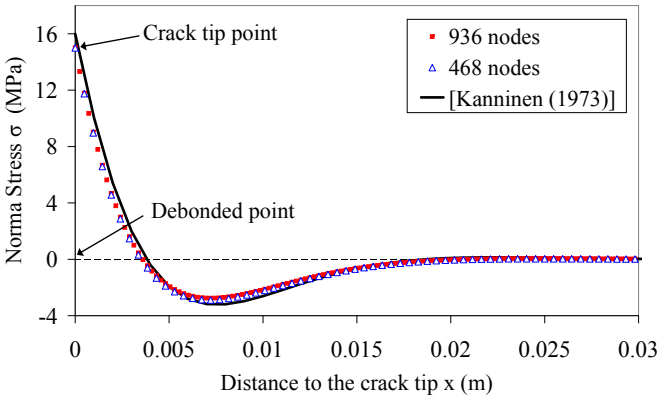

Figure 9: Normal stresses σ near the crack tip along the bonded zone, for a load step with P=29.7N, d=35.4mm and a=146.6mm.

In view of Lenci's expression, Eq. 27, for the local normal stresses along the bonded interface part close to the crack tip in a particular problem, and taking into account a general singularity analysis of a crack in presence of spring boundary conditions

[1] In the present orthotropic case the parameter λ in [Kanninen (1973)] is defined as $\lambda^4 = \frac{6k_n}{E_x(t/2)^3}$.

in [Sinclair (1996)], it appears that the first terms in the asymptotic expansion of the normal stresses take the form:

$$\frac{\sigma}{\sigma_c} = c_0 + c_1 \xi \left[\ln(\xi) + c_2\right]. \tag{28}$$

Thus, these stresses are bounded, but their gradient has a logarithmic singularity at the crack tip. In this sense, it is noteworthy that the local numerical BEM solution for normal stresses in the present G_{Ic} specimen near the crack tip fits this expression very well. In Fig. 10, the normalized stresses σ/σ_c represented as a function of ξ are compared with the following fitted expression:

$$\frac{\sigma}{\sigma_c} = 1.0038 + 9.9132\xi \left[\ln(\xi) - 1.0991\right] \tag{29}$$

obtained from Eq. 28 by applying the least square method to the first nodes with $\xi < 0.012$. An excellent agreement between the BEM solution and the fitted asymptotic expression can be observed, and in addition to $c_0 \cong 1$ also $c_2 \cong -1$ in agreement with Eq. 27. Notice that this asymptotic behavior is applicable for the local solution near the crack tip only.

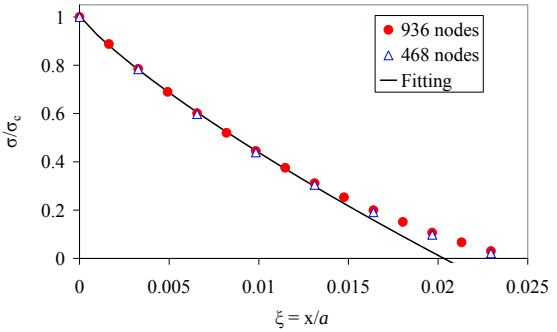

Figure 10: Fitting of the BEM normalized local stress solution by an analytic expression (Eq. 29), for a load step with P=29.7N, d=35.4mm and a=146.6mm.

The deformed shape obtained for the same load step as defined before is depicted in Fig. 11(a). A detailed view of the deformed shape obtained with the BEM code is shown in Fig. 11(b). The different zones where the springs are broken, and where the springs are in traction or in compression, are clearly indicated in the plot.

5.3 Experimental and numerical load - displacement diagrams

As can be observed in Fig. 12, the numerical results obtained provide a good approximation of the experimental results. Therefore, the use of the weak interface formulation seems to be a promising approach to model composite adhesive joints.

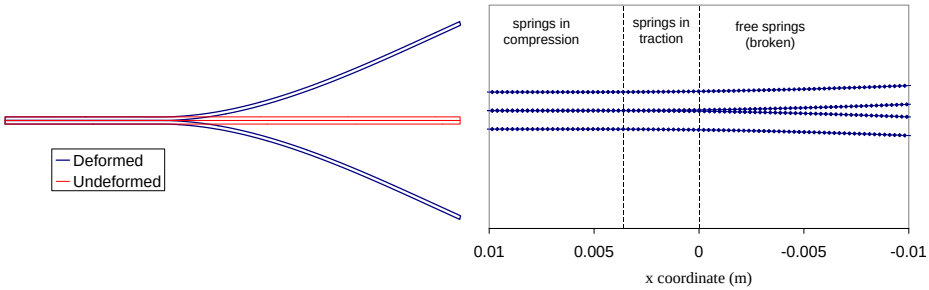

(a) (b)

Figure 11: (a) Numerical deformed shape obtained, (b) Detail of the deformed shape at the vicinity of the crack tip.

It is important to mention that in the experimental curve an unloading and a reloading are done because the laboratory standard required them; this behavior was not simulated due to its irrelevant effect on the numerical solution.

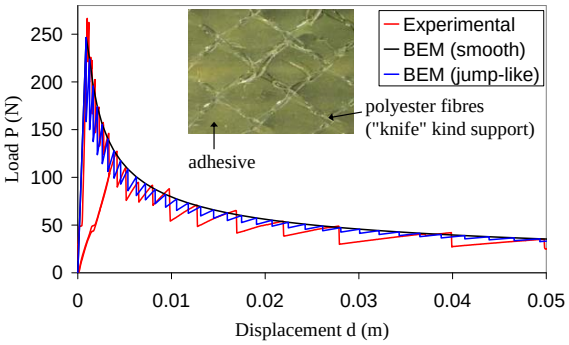

Figure 12: Comparison between the experimental and numerical load - displacement diagrams and a detail of the polyester support of the adhesive used.

Changing the non-linear conditions node by node can make the crack propagation very smooth (especially for fine meshes), in contrast with the experimental evidence found in some industrial adhesives that show crack growth by small but clearly finite jumps. For this specific kind of adhesive (especially the ones that have a "knife" kind support, see Fig. 12) the end of a load step can be defined by a situation where the normal and tangential stiffnesses of a fixed number of consecutive nodes are set to zero. This number of nodes are related to the size of the rhombus-like mesh support of the adhesive, Fig. 8, and the marks observed in the experimental results, Fig. 7. In the results shown in Fig. 12, in the jump-like curve obtained, 15 nodes were opened in each load step, which corresponds to approximately 5 times half of the width of a rhombus and also corresponds to the first distances between marks, Fig. 7. As can be seen from the BEM results, the jumps

remain constant while the jumps in the experimental results become larger. Nevertheless, the most important result is that the model is able to catch the failure load as well as the energy dissipated during the debonding process, by means of a unique critical parameter (σ_c or, equivalently, G_{Ic} see Eq. 7) together with the stiffness parameter k_n.

5.4 Non-symmetric DCB specimen

In order to see the capability of the mixed mode failure criterion proposed in Section 2.2, a non-symmetric DCB specimen has been studied numerically. The composite laminate and adhesive layer are assumed to have the same properties as in the previous section. The geometry of the specimen is almost the same as that depicted in Fig. 6, except for the thickness of the laminates taken as $t/2$ and t (one laminate two times thicker than the other). In Fig. 13 the global load - displacement response is shown, and compared with the previously studied symmetric DCB specimen. As can be seen, the failure load necessary to start the crack growth is a little higher. Another important effect is the presence of tangential stresses along the interface, leading to values of the fracture mode mixity angle ψ_G in the following interval $7.15^\circ < \psi_G < 9.01^\circ$ for 12mm$< a <$ 208mm respectively.

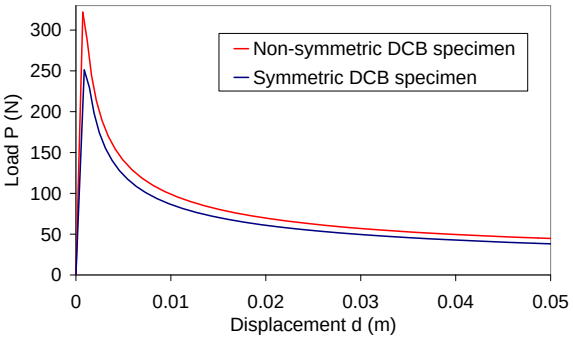

Figure 13: Numerical load - displacement diagrams for a symmetric and non-symmetric DCB specimen (bonded joint).

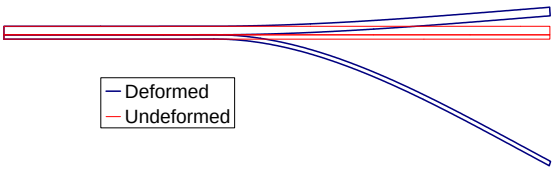

Figure 14: Numerical deformed shape obtained for a non-symmetric DCB specimen (bonded joint).

In Fig. 14 the deformed shape obtained is shown for a load step with P=46.48N, d=45.8mm and a=134.6mm.

6 Conclusions

The presence of a crack at a weak interface, which represents a simple model of a thin adhesive layer, is analyzed in the present work. First the governing integral equation for a pressurized crack at the weak interface between identical orthotropic half planes has been deduced. A new dimensionless characteristic structural parameter δ was introduced in this governing integral equation . It relates adhesive-layer stiffness to the adherent stiffness, taking into account crack length. Then, the problem of a pressurized crack has been solved by the collocational BEM. An excellent agreement has been obtained between the numerical results by the present BEM code and those shown in [Lenci (2001)].

An important novelty is that in the present work not only is stress and displacement numerical solution for a crack at a weak interface presented (Section 4), but also the crack growth along the weak interface is modeled using a mixed mode fracture criterion for an adhesive thin layer modeled by linear-elastic brittle traction-displacement law.

Noteworthy, in accordance with the model used, is the bounded character of stresses along the weak interface, the maximum value of stresses being achieved at the crack tip. The spring constitutive law introduced and included in the incremental algorithm of the BEM code has the advantage of being independent of the number of springs used in the interface. An analytic expression for the local solution of normal tractions at the crack tip, deduced in the singularity analysis of the weak interface by Lenci in a particular problem for isotropic half-planes, has been successfully compared with the present numerical solution for orthotropic laminates.

As shown by the numerical results presented in Section 5, the weak interface formulation modeled by a spring distribution correctly describes the behavior of adhesive joints used in the aeronautical industry. From laboratory tests and fractographic analysis it has been concluded that the jumps appearing in the experimental load - displacement curve are caused by the polyester support of the adhesive resin. The experimental and numerical comparison presented in Section 5 corresponds to opening mode I due to symmetry configuration of the specimen. Nevertheless, the present implementation of the weak interface model allows for a similar analysis of non-symmetric configurations of bonded adhesive joints leading to a mixed fracture mode as studied numerically in Section 5.4. It has been proved that the real behavior of an adhesive layer with a polyester support that joins two unidirectional laminates can be approximated very well by means of BEM and a distribution of

springs which follow a linear elastic-brittle constitutive law, by adjusting the parameters of the discrete model (k_n, σ_c, and the number springs that break in a load step). This fact will make it possible to predict the real behavior of structures that include similar adhesive joints by the model developed here. The formulation introduced here for the mixed mode crack growth along a weak interface will be useful for analysis of the fiber-matrix debonding under transversal load that will be presented in a forthcoming paper. It can be also useful for analysis of interlaminar fracture toughness test of non-symmetric adhesively bonded joints with different laminas, due to different stacking sequence and/or lamina thickness or analysis of delamination cracks in cross ply laminates [Blázquez, Mantič, París, and McCartney (2008)]. The results obtained in this work can also be considered a starting point for a study of adhesively bonded joints used in the aeronautics industry including adhesive supports of different kinds.

Acknowledgement: The authors are grateful to Ms. María Eugenia Jiménez for providing the previous numerical and experimental results of the G_{Ic} test. The authors thank the anonymous referee for the useful comments and for drawing their attention to the analytical solution of a beam on a Winkler foundation. The work was supported by the Junta de Andalucía (Projects of Excellence TEP-1207, TEP-2045 and TEP-4051), the Spanish Ministry of Education and Science through Projects TRA2005-06764 and TRA2006-08077.

References

Agrawal, A.; Karlsson, A. M. (2007): On the reference length and mode mixity for a bimaterial interface. *Journal of Engineering Materials and Technology*, vol. 129, pp. 580–587.

Airbus (2006): Carbon Fibre Reinforced Plastics. Determination of fracture toughness energy of bonded joints. Mode I. G1C. Issue 1. *AITM 1-0053*.

Bank-Sills, L.; Ashkenazi, D. (2000): A note on fracture criteria for interface fracture. *International Journal of Fracture*, vol. 103, pp. 177–188.

Blázquez, A.; Mantič, V.; París, F.; Cañas, J. (1996): On the removal of rigid body motions in the solution of elastostatic problems by direct BEM. *International Journal for Numerical Methods in Engineering*, vol. 39, pp. 4021–4038.

Blázquez, A.; Mantič, V.; París, F.; McCartney, L. N. (2008): Stress State characterization of delamination cracks in [0/90] symmetric laminates by BEM. *International Journal of Solids and Structures*, vol. 45, pp. 1632–1662.

Blázquez, A.; París, F.; Mantič, V. (1998): BEM solution of two-dimensional contact problems by weak application of contact conditions with nonconforming

discretizations. *International Journal of Solids and Structures*, vol. 35, pp. 3259–3278.

Camacho, G.; Ortiz, M. (1996): Computational modelling of impact damage in brittle materials. *International Journal of Solid and Structures*, vol. 33, pp. 2899–2938.

Camanho, G.; Dávila, C.; de Moura, M. (2003): Numerical simulation of mixed-mode progressive delamination in composite materials. *Journal of Composite Materials*, vol. 37, pp. 1415–1438.

Carpinteri, A. (1989): Cusp catastrophe interpretation of fracture instability. *Journal of the Mechanics and Physics of Solids*, vol. 37, pp. 567–582.

Carpinteri, A. (1989): Post-Peak and Post-Bifurcation Analysis on Cohesive Crack Propagation. *Engineering Fracture Mechanics*, vol. 32, pp. 265–278.

Carpinteri, A.; Cornetti, P.; Pugno, N. (2009): Edge debonding in FRP strengthened beams: Stress versus energy failure criteria. *Engineering Structures*, vol. 31, pp. 2436–2447.

Dollhofer, J.; Beckert, W.; Lauke, B.; Schneider, K. (2001): Fracture mechanics characterization of mixed-mode toughness of thermoplast/glass interfaces (brittle/ductile interfacial mixed-mode fracture). *Journal of Adhesion Science and Technology*, vol. 15, pp. 1559–1587.

Erdogan, F. (1997): *Fracture mechanics of interfaces, In: Damage and Failure of Interfaces*. Balkema Publishers: Rotterdam.

Evans, A. G.; Rühle, M.; Dalgleish, B. J.; Charalambides, P. G. (1990): The fracture energy of bimaterial interfaces. *Metallurgical Transactions A*, vol. 21, pp. 2419–2429.

Geymonat, G.; Krasucki, F.; Lenci, S. (1999): Mathematical analysis of a bonded joint with a soft thin adhesive. *Mathematics and Mechanics of Solids*, vol. 4, pp. 201–225.

Graciani, E.; Mantič, V.; París, F.; Blázquez, A. (2005): Weak formulation of axi-symmetric frictionless contact problems with boundary elements: Application to interface cracks. *Computer & Structures*, vol. 83, pp. 836–855.

Hilleborg, A.; Modeer, M.; Petersson, P. (1976): Analysis of a crack formation and crack growth in concrete by fracture mechanics and finite elements. *Cement and Concrete Research*, vol. 6, pp. 773–782.

ISO (2001): Fibre-reinforced plastic composites – Determination of mode I interlaminar fracture toughness, G_{IC}, for unidirectionally reinforced materials. *ISO 15024*.

Jiménez, M. E.; Cañas, J.; Mantič, V.; Ortiz, J. E. (2007): Numerical and experimental study of the interlaminar fracture test of composite-composite adhesively bonded joints. (in Spanish). *Materiales Compuestos 07, Asociación Española de Materiales Compuestos, Universidad de Valladolid*, pp. 499–506.

Kanninen, M. F. (1973): An augmented double cantilever beam model for studying crack propagation and arrest. *International Journal of Fracture*, vol. 9, pp. 83–92.

Kočvara, M.; Mielke, A.; Roubíček, T. (2006): A Rate-Independent Approach to the Delamination Problem. *Mathematics and Mechanics of Solids*, vol. 11, pp. 423–427.

Lekhnitskii, S. G. (1981): *Theory of Elasticity of an Anisotropic Body*. Mir Publishers: Moscow.

Lenci, S. (2001): Analysis of a crack at a weak interface. *International Journal of Fracture*, vol. 108, pp. 275–290.

Liang, Y.-M.; Liechti, K. M. (2005): Toughening mechanisms in mixed-mode interfacial fracture. *International Journal of Solids and Structures*, vol. 32, pp. 957–978.

Maier, G.; Frangi, A. (1998): Symmetric boundary element method for 'discrete' crack modelling of fracture processes. *Computer Assisted Mechanics and Engineering Sciences*, vol. 5, pp. 201–226.

Mantič, V. (2008): Discussion: "On the reference length and mode mixity for a bimaterial interface". *Journal of Engineering Materials and Technology*, vol. 130, pp. 045501:1–2.

Mantič, V.; Blázquez, A.; Correa, E.; París, F. (2006): *Analysis of interface cracks with contact in composites by 2D BEM. In: Fracture and damage of composites, Series: Advances in fracture mechanics*. WIT Press: Southampton, Boston.

Mantič, V.; París, F. (1995): Explicit formulae of the integral kernels and C-matrix in the 2D Somigliana identity for orthotropic materials. *Engineering Analysis with Boundary Elements*, vol. 15, no. 3, pp. 283–288.

Needleman, A. (1987): A continuum model for void nucleation by inclusion debonding. *Journal of Applied Mechanics*, vol. 54, pp. 525–532.

París, F.; Cañas, J. (1997): *Boundary Element Method, Fundamentals and Applications*. Oxford University Press: Oxford.

Roubíček, T.; Scardia, L.; Zanini, C. (2009): Quasistatic delamination problem. *Continuum Mechanics and Thermodynamics*, vol. 21, pp. 223–235.

Sinclair, G. B. (1996): On the influence of cohesive stress-separation laws on elastic stress singularities. *Journal of Elasticity*, vol. 44, pp. 203–221.

Swadener, J. G.; Liechti, K. M.; de Lozanne, A. L. (1999): The intrinsic toughness and adhesion mechanisms of a glass/epoxy interface. *Journal of Mechanics and Physics of Solids*, vol. 47, pp. 223–258.

Távara, L.; Mantič, V.; Graciani, E.; Cañas, J.; París, F. (2008): BEM model of mode I crak propagation along a weak interface applied to the interlaminar fracture test of composites. *Advances in Boundary Element Techniques IX, EC Ltd, Eastleight*, pp. 461–466.

Távara, L.; Mantič, V.; Graciani, E.; Cañas, J.; París, F. (2009): Analysis of a crack in a thin adhesive layer between orthotropic materials applied to composite interlaminar fracture toughness test. *Composites 2009, 2nd ECCOMAS Thematic Conference on the Mechanical Response of Composites, London, UK*.

Ting, T. C. T. (1996): *Anisotropic Elasticity Theory and Applications*. Oxford University Press: Oxford.

Wen, P. (1992): The elastic solution of concentrated force acting in orthogonal anisotropic half-plane and constant element fundamental formulae of boundary element method. *Applied Mathematics and Mechanics*, vol. 13, pp. 1163–1172.